Acoustic surface wave generation over rigid cylinder arrays on a rigid plane

Acoustic surface wave generation over rigid cylinder arrays on a rigid plane

David L. Berry[a)]
Departamento de Física, Universidade de Évora, 7002-554 Évora, Portugal

Shahram Taherzadeh and Keith Attenborough
Faculty of Science, Technology, Engineering and Mathematics, Open University, Walton Hall, Milton Keynes, MK7 6AA, United Kingdom

(Received 20 December 2018; revised 27 August 2019; accepted 5 September 2019; published online 2 October 2019)

Propagation of an airborne acoustic pulse from a point source above an array of regularly spaced rigid cylinders on a rigid plane has been investigated using a two-dimensional multiple scattering theory. Time domain simulations show a main arrival and a separate delayed "tail." Fourier analysis of the tail shows that, for a sufficiently sparse array of cylinders, it is composed of a series of spectral peaks resulting from constructive interference consistent with Bragg diffraction theory and amplitudes depending on the spacing and size of the cylinders. For increasingly compact distributions of cylinders, the lowest frequency peak is dominated by a quarter wavelength "organ pipe" or "gap" resonance in the space between the cylinders. Simulated pressure maps show that there is a transition region in the acoustic field with an extent that depends on the spacing and size of the cylinders. Beyond this region, individual gap resonances combine to create a field that declines exponentially with height, consistent with the behaviour of a surface wave. Data from measurements of acoustic pulses above copper cylinders on rigid fibreboard under anechoic conditions demonstrate some of the predicted characteristics.
https://doi.org/10.1121/1.5126856

[OU] Pages: 2137–2144

I. INTRODUCTION

It is generally accepted that if an acoustic airborne source is located near a plane surface, an acoustic surface wave may be generated depending upon the nature of that surface. That is, instead of acoustic energy being reflected from or transmitted into the surface, some energy remains just above and propagates along that surface. This is the acoustic analogue of the Rayleigh wave—the surface wave that propagates independently along the surface of solids produced by, for example, localised impact, piezo-electric transduction, and earthquakes. A surface with an impedance in which the imaginary part sufficiently exceeds the real part is an example of this type of surface. Another is a rough surface composed of a periodic or aperiodic structuring on a plane where the mean spatial period of the structuring is smaller than the wavelength (this surface can be considered to be a form of meta-surface).[1] Whatever the type of surface, a surface wave generated by an airborne source near that surface is characterised by specific properties; it undergoes cylindrical spreading with increasing range along the plane, exponential decay with increasing height above the plane, and a reduced phase velocity $v < c$ where c is the velocity of sound in air. The objective of this study is to investigate the generation of airborne surface waves during propagation from a point source over an array of regularly spaced rigid cylinders on a rigid plane.

The theoretical basis for the generation of acoustic surface waves above an impedance plane has been investigated by many workers including Thomasson[2] who showed that if a surface has an impedance with an imaginary part much larger than the real part, an acoustic surface wave can be generated when the incident wave is at or near grazing incidence. Later, Raspet and Baird[3] demonstrated that such a surface wave is an independently propagating wave. Also, it was shown by Tolstoy[4,5] and Twersky[6] that acoustic surface waves can also be generated by rough surfaces. The existence of acoustic surface waves has been demonstrated experimentally over arrays of thin aluminium strips mounted on a rigid sheet of plywood,[7] lattices of square cavities constructed from overhead lighting panels mounted on a wooden board,[8] rectangular strips on a hard surface[9] and a comb-like structure.[10,11] Allard, Lauriks, and Kelders[12–14] investigated ultrasonic surface wave generation over triangular-grooves, rectangular grooves, a doubly periodic grating, and honeycomb surfaces. Daigle *et al.*[15] showed that a separate wave can be produced over a surface constructed from commercial overhead lighting panels, but the measurements did not show as much separation as predicted. Most of these experimental studies provide evidence for the existence of surface waves over rough surfaces but do not propose mechanisms that lead to their generation. Previous studies have investigated the propagation of

[a)]Electronic mail: dberry@uevora.pt

acoustic waves above randomly and regularly structured surfaces using numerical techniques such as boundary element methods[16] and boss theories.[17] Other studies have used a multiple scattering theory (MST) approach,[18,19] which provided good agreement between the model predictions and measurements for semi-cylindrical elements (although agreement for other shapes, such as triangular and rectangular elements, were less satisfactory).

To explore the characteristics of the surface wave generated by a rough surface and the possible mechanisms that lead to its generation, a model surface was necessary which had rough surface characteristics that could be easily modified, and which could be modelled simply and efficiently. Another requirement was that it could be constructed and tested in an acoustics laboratory. A surface composed of an acoustically rigid plane surface with acoustically rigid cylinders horizontally placed on it and oriented perpendicularly to the direction of propagation satisfied these requirements. The simulations for propagation above such a surface presented in this study are based on the MST formulation of Krynkin *et al.*,[19] an outline of which is presented. If such a surface does in fact generate a surface wave then, for an airborne pulse emitted near to the surface, it will manifest itself as a separate delayed "tail" after the (direct and plane-surface reflected) main arrival. Isolating this tail in the time domain and subsequently analysing it in the frequency domain could reveal possible mechanisms that lead to its generation. Two possible mechanisms are proposed and presented in this study. The first is Bragg diffraction which occurs when two diffracted plane waves interfere destructively or constructively depending on the difference in their path lengths. The second is a resonance effect generated in the gaps between the cylinders of the array, similar to "organ pipe" resonance. Simulations that investigate these two competing mechanisms are presented with a particular focus on the influence of the geometry (cylinder centre-to-centre spacing, cylinder diameters, etc.). This study also presents a comparison of these simulations with measurements above a model surface of evenly spaced copper cylinders on an acoustically hard fibreboard under controlled conditions in an anechoic chamber.

In Sec. II we describe the multiple scattering theory for the spatial dependence of the acoustic pressure waveforms produced for different source–receiver geometries and different configurations and sizes of acoustically rigid cylinders on a rigid plane. Using this theory, we explore, in Sec. III, how such a rough surface affects the propagation of acoustic pulses—and in this case, the propagation of delta pulses of infinitely short length corresponding to a flat, infinitely wide, frequency spectrum. Section IV describes the experimental procedures and laboratory arrangements used in this study and presents comparisons of measured pulses over arrays of copper tubes on a rigid fibreboard board with simulations. Finally, Sec. V draws conclusions and completes this study.

II. THE MULTIPLE SCATTERING MODEL

The characteristics of sound propagating over cylinders on a rigid plane has been explored here using a treatment similar to that of Krynkin *et al.*[19] who determined the acoustic insertion loss due to two dimensional periodic arrays of circular cylinders parallel to a nearby surface. Bashir *et al.*[16] have shown that this semi-analytical theory enables good agreement with measurements over arrays of semi-cylinders on a rigid plane.

Consider a cylindrical wave from a point source located in air characterised by sound speed $c = 343$ m/s and density $1.2\,\mathrm{kg/m^3}$ incident on an array of N identical rigid cylinders, each of radius a, placed on a flat rigid plane and arranged perpendicularly to the direction of propagation —see Fig. 1. The polar coordinates at the receiver in the Cartesian reference frame (Ox, Oy) are represented by (r, θ), and the polar coordinates at the receiver in the reference frame $(O_j x, O_j y)$ centred at the jth cylinder centre, $O_j(x_j, y_j)$, are represented by (r_j, θ_j).

The total field, P, at the receiver is the sum of a direct field contribution, a contribution from the plane boundary and a contribution from the cylindrical scatterers and must satisfy the Helmholtz equation in polar coordinates:

$$\nabla^2 P + k_0^2 P = 0, \tag{1}$$

where

$$\nabla^2 = \frac{1}{r}\frac{\partial}{\partial r}\left(r\frac{\partial}{\partial r}\right) + \frac{1}{r^2}\frac{\partial^2}{\partial \theta^2}$$

is the Laplacian and k_0 is the wave-number exterior to the cylinders. Equation (1) is solved in conjunction with radiation conditions,

$$\frac{\partial P}{\partial r} - ik_0 P = o\left(r^{-1/2}\right), \quad \text{as } r \to \infty, \tag{2}$$

and with the Neumann condition imposed on the rigid plane and on the cylinders, i.e.,

$$\frac{\partial P}{\partial n} = 0. \tag{3}$$

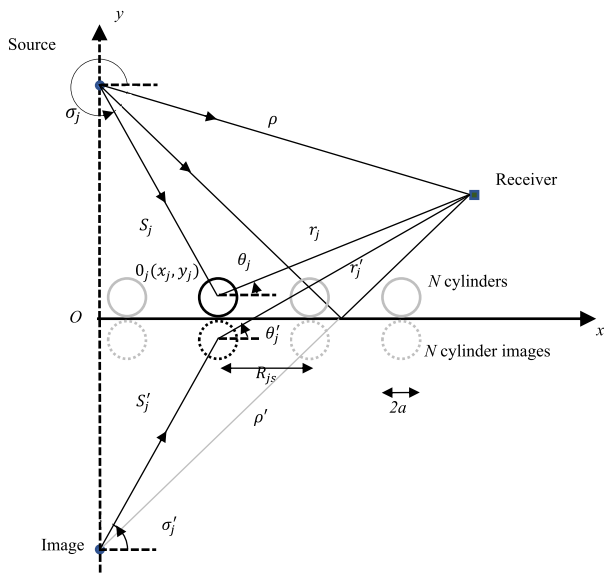

FIG. 1. (Color online) Geometry used for theoretical development.

Assuming a direct field represented by a Hankel function $H_0^{(1)}(k_0\rho)$, where ρ is the source–receiver distance (see Fig. 1), a plane boundary reflected wave $H_0^{(1)}(k_0\rho')$ represented by the wave from an image source, where ρ' is the image source–receiver distance, and a scattered field decomposed into a sum of the contributions from the N cylinders and N cylinder images, the following expression can be developed for the total field above the array of cylinders:

$$P = H_0^{(1)}(k_0\rho) + H_0^{(1)}(k_0\rho') + \sum_{j=1}^{N}\sum_{n=-\infty}^{\infty} A_n^j Z_n^j H_n^{(1)}(k_0 r_j) e^{in\theta_j} + \sum_{j=1}^{N}\sum_{n=-\infty}^{\infty} A_n^j Z_n^j H_n^{(1)}\left(k_0 r_j'\right) e^{-in\theta_j'}, \quad (4)$$

where $H_n^{(1)}(\,)$ are Hankel functions of the first kind and order n and A_n^j, $n \in \mathbb{Z}$, $j = 1 \ldots N$ are unknown amplitudes. For acoustically rigid cylinders, the term Z_n^j is defined as

$$Z_n^j = \frac{J_n'(k_0 a)}{H_n'(k_0 a)}, \quad (5)$$

where $J_n'(\,)$ is the derivative of the Bessel function of order n and $H_n'(\,)$ is the derivative of the Hankel function of the first kind of order n with respect to polar coordinate r. This leads to the infinite system of equations for unknown coefficients A (for details see Krynkin *et al.*[19]),

$$A_m^s + \sum_{n=-\infty}^{\infty}\left\{\sum_{\substack{j=1\\ j\neq s}}^{N} A_n^j Z_n^j H_{n-m}^{(1)}(k_0 R_{js}) e^{i(n-m)\alpha_{js}} + \sum_{j=1}^{N} A_n^j Z_n^j H_{n+m}^{(1)}(k_0 R_{js}) e^{i(n+m)\alpha_{js}'}\right\} = -H_m^{(1)}(k_0\rho) e^{-im\sigma_\rho} - H_m^{(1)}(k_0\rho') e^{-im\sigma_{\rho'}}, \quad (6)$$

with $m \in Z$ and $s = 1, \ldots, N$. In Eq. (6) the summation is taken over both real and image cylinders to take account of interaction between real and image objects. These interactions account for scattering of ground reflected waves and reflection from the ground of scattered waves. The source terms on the right-hand side are the source and its image below the rigid plane. To determine the coefficients A_n^j, the infinite summation is truncated to $-M$ to M, where the value of M is set to 6 (for further details see Ref. 14). The procedure for determining the total pressure field P at a certain point above the cylinder array using this multiple scattering approach requires solving the system of Eq. (6) and determining the pressure by summation using Eq. (4) together with direct and boundary-reflected terms.

Using this treatment, the propagation of a short acoustic pulse over a cylinder array configuration can be predicted theoretically and the measurements, to be discussed later, can be compared directly with predictions. To determine the signal $p_{Final}(t)$ at a certain point above the cylinder array, given a signal $p_{Ref}(t)$ at the source, discrete Fourier transform (DFT) was used to determine $P_{Ref}(f)$ from $p_{Ref}(t)$ and the final signal was determined from

$$P_{Final}(f) = P(f)\, P_{Ref}(f). \quad (7)$$

An inverse DFT was subsequently used to obtain the final signal $p_{Final}(t)$ from $P_{Final}(f)$. The reference signal was sampled at 13.25 μs and a rectangular window of 4096 sample points was used for the analysis, which provided a sufficiently extensive time interval to encompass the main pulse signal and the pulse "tail." The spectral resolution of the DFT is 0.054 Hz, considered sufficient to represent the pulse spectrum accurately.

Finally, it is useful to know how the total pressure at a certain point above the cylinder array varies compared to the pressure above a rigid plane, given by

$$P_{RP} = H_0^{(1)}(k_0\rho) + H_0^{(1)}(k_0\rho') \quad (8)$$

and we determine the relative sound pressure level (SPL) with reference to the rigid plane using

$$SPL = 20\log_{10}\left|\frac{P_{Final}(f)}{P_{RP}(f)}\right|. \quad (9)$$

III. IMPULSE RESPONSE FOR THE CYLINDER ARRAY

To determine the influence of the cylinder array on the propagation of an acoustic pulse from a cylindrical source, especially to understand the spectral content of signal at a certain point above the array, the simulations presented in this section were carried out using the Dirac delta function,

$$P_{Ref}(t) = \begin{cases} 1, & t = 0 \\ 0, & otherwise. \end{cases} \quad (10)$$

The advantage of using such a reference pulse in simulations is that its frequency spectrum is flat and infinitely wide. This means that pressure field determined using Eq. (7) will be independent of the frequency content of the input pulse and any variations in the spectral content of the signal above the array will be the direct result of the array.

Figure 2 shows the results of simulations for propagation over a cylinder array configuration where the cylinders are positioned regularly and symmetrically about the point of specular reflection at a cylinder centre-to-centre spacing of 5 cm, corresponding to 20 cylinders between source and receiver. The source–receiver separation is 1 m and both the source and receiver heights are 5 cm. Figure 2(a) shows a main pulse arrival at 2.9 ms (corresponding to a sound speed of 343 m/s) followed by a "tail" which persists for an additional 5 to 10 ms. The spectrum of this tail [Fig. 2(b)] is dominated by a peak at 2.7 kHz. The three other peaks at 5.8, 9.6, and 13.6 kHz have much lower magnitudes. The frequencies of these four peaks correspond approximately with the frequencies of the four minima in the sound pressure level spectrum shown in Fig. 2(c).

This example demonstrates how the spectra of the pulse tails are predicted to depend upon the cylinder configuration. Consider now the effects of symmetrically altering cylinder centre-to-centre spacing and cylinder size.

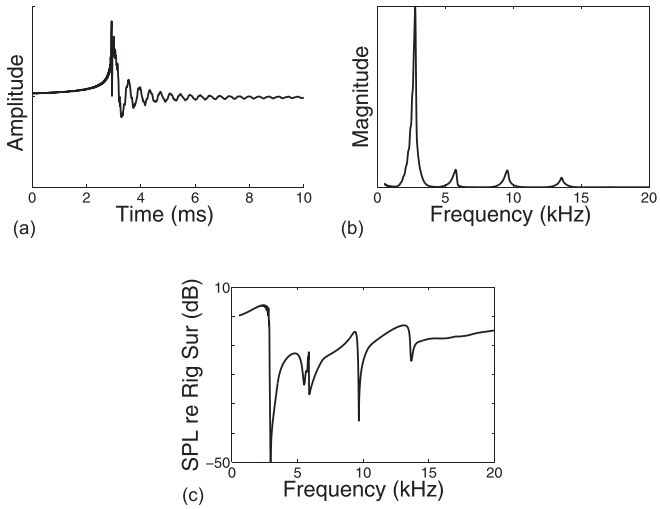

FIG. 2. (a) Example pulse, (b) its tail spectrum and (c) sound pressure level spectrum relative to a rigid surface calculated for propagation over cylinder array (cylinder diameter 1.5 cm) for an input delta pulse; source–receiver separation = 1.0 m, source and receiver heights = 5 cm; cylinder centre-to-centre spacing = 5 cm (20 cylinders).

Figure 3(a) presents hidden line plots of pulse tail spectra as a function of cylinder centre-to-centre spacing for a fixed cylinder diameter (1.5 cm). When the spacing is small, the pulse tail spectrum is dominated by a peak at ~3 kHz. As the spacing increases, the frequency of this peak decreases to ~1500 Hz. The frequencies of the other lower-magnitude peaks also decrease smoothly with increasing separation.

According to Bashir *et al.*[9] certain maxima observed in sound pressure level spectra over periodically spaced roughness elements are influenced by the spacing of the roughness elements. This influence was attributed to Bragg diffraction which occurs when two diffracted plane waves interfere destructively or constructively depending on the difference in their path lengths. The frequencies at which these interferences occur are the Bragg frequencies,

$$f_{br} = \frac{c_0 n}{2R \sin\gamma}, \quad n = 1, 2, 3, \ldots, \tag{11}$$

where c_0 is the speed of sound in air, R is the cylinder centre-to-centre spacing, and γ is the angle of incidence. This assumes the scattering elements to be of infinitesimal size and, therefore, that the Bragg frequency is independent of the size of the scattering elements.

Figure 3(b) presents a comparison of the frequencies of the first four maxima taken from Fig. 3(a) with predicted first- to fourth-order Bragg frequencies corresponding to $n = 1$, 2, 3, and 4 as a function of cylinder spacing, calculated using Eq. (10). Figure 3(b) shows that there is reasonable agreement of the frequencies of the first peak (circles) with the Bragg diffraction equation (dashed line) for large cylinder spacings but this agreement breaks down when the spacing is small, i.e., when the cylinders are close together. However, Fig. 3(b) shows that the agreement with predictions according to Bragg diffraction improves with the diffraction order (even for small cylinder spacings).

Another mechanism must be responsible for the difference between the first maximum and the first order Bragg diffraction maximum. Whatever the effect is, it is certainly stronger than that caused by diffraction. Perhaps the clue lies in the cylinder configurations. At large cylinder separations (>cylinder diameter), the cylinders are acting as individual diffraction elements and with the appropriate geometry, Bragg diffraction occurs. However, at much smaller cylinder spacings—approaching a value of a cylinder diameter—the centre-to-centre-cylinder gap width and height are similar. In this case, the cylinders can no longer be considered infinitesimal scattering elements and the gaps between the cylinders will play an important role in the sound propagating over the cylinder array. When the cylinders are close together the gaps between adjacent cylinders (although resembling a concave lens) have rigid sides, a rigid base and

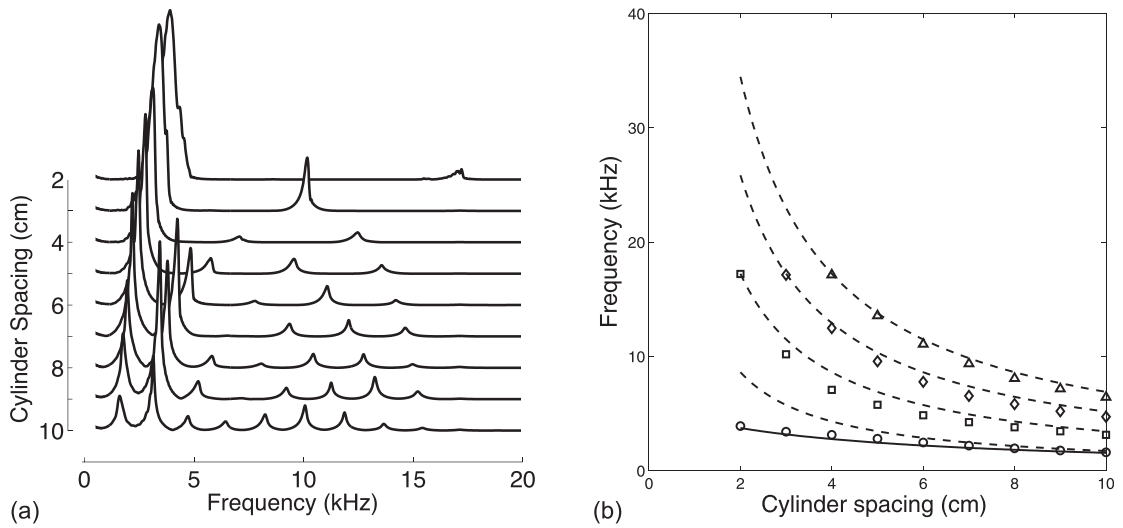

FIG. 3. (a) Spectra of pulse tails calculated over a cylinder array (cylinder diameter 1.5 cm) for cylinder centre-to-centre spacings ranging from 2 to 10 cm for an input delta pulse. The source–receiver separation = 1.0 m, source and receiver heights = 5 cm. (b) Variation of the frequency of the first (circles), second (squares), third (diamonds), and fourth (triangles) maxima of the plots in (a) compared with the equivalent Bragg frequencies calculated using Eq. (11) (dashed lines) and the gap resonance frequencies calculated using Eq. (12b) (solid line) (with $C = 7$ cm).

TABLE I. Frequency of first gap resonance, f_{OP} for different values of end correction, C ranging from $0.31d$ to $\pi/4$ d calculated using Eq. (12b). The effective diameter of the organ pipe, d, is taken to be the cylinder-to-cylinder spacing, 0.02 m; the effective length of the organ pipe is taken to be $2a$, 0.015 m.

C (m)	f_G (kHz)
0.0062 ($= 0.31 \times 0.02$)	4.04
0.0070 ($= 0.35 \times 0.02$)	3.90
0.0080 ($= 0.40 \times 0.02$)	3.73
0.0100 ($= 0.50 \times 0.02$)	3.43
0.0120 ($= 0.60 \times 0.02$)	3.18
0.0140 ($= 0.70 \times 0.02$)	2.96
0.0157 ($= \pi/4 \times 0.02$)	2.79

are open at the top. So, there may be resonances similar to so-called "organ pipe" resonances occurring.

For a cylindrical organ pipe of length L, diameter d, and closed at one end, quarter wavelength resonances are given by[20]

$$f_{OP} = \frac{c_0 n}{4(L + C)}, \quad n = 1, 3, 5, \ldots, \tag{12a}$$

where C is an end correction which can take a value between $(0.31d)$ to $(\pi d/4)$. If the length of the organ pipe is taken to be $L = 2a$, and its effective diameter is taken to be $d = R$, where R is the cylinder centre-to-centre spacing, then the frequency of the first "gap" resonance is

$$f_G = \frac{c_0}{4(2a + C)}. \tag{12b}$$

Table I shows the variation of this first gap resonance for different values of the end correction, C, for the smallest value of cylinder centre-to-centre spacing considered here ($d = 2$ cm). Using an end correction of 7 mm, a value that falls between the limits proposed by Pierce,[20] Fig. 3(b) shows the variation of the gap frequency as a function of cylinder centre-to-centre spacing and demonstrates that Eq. (12b) predicts the frequencies of the first tail maxima from the multiple scattering theory.

Clearly, depending on the cylinder diameters and the cylinder-to-cylinder spacing, there are simultaneous contributions from Bragg diffraction and the gap resonance for propagation over regularly spaced cylinder arrays. Further confirmation of the latter effect can be made if we look at hidden line plots of predicted tail spectra as a function of cylinder diameter for a fixed cylinder centre-to-centre spacing [see Fig. 4(a)].

For small diameter cylinders (~1–3 mm) and up to a frequency of 20 kHz, the tail spectra include two maxima at 8.6 kHz and 17.1 kHz which approximately coincide with the predicted frequencies for the first and second order Bragg diffraction frequencies calculated using Eq. (10). However, the second peak diminishes with increasing cylinder diameter up to ~10 mm and its frequency also reduces to ~14 kHz, but subsequently returns to its original value with a further increase in cylinder diameter; this is also accompanied by an increase in magnitude. This is not the case for the first maximum. With increasing cylinder diameter, its magnitude increases and shifts to lower frequencies—to a value of 3.9 kHz for cylinder diameters of 1.5 cm. Figure 4(b) shows the variation of the frequency of these maxima as a function of cylinder diameter. These frequencies are predicted using Eq. (12b), with a value of the end correction $C = 0.007$ m as used in Fig. 3(b). As expected, for small cylinder diameters, the organ pipe resonance no longer dominates, and the frequency of the maxima are predicted using Bragg diffraction.

Figures 3 and 4 have shown that the maxima in the tail spectra can be explained using either Bragg diffraction or gap resonance. This indicates that the generation of these maxima are a result of the regularity of the arrangement of the cylinders between source and receiver. If this regularity were removed, i.e., if the cylinders were arranged irregularly between source and receiver, then the conditions for Bragg

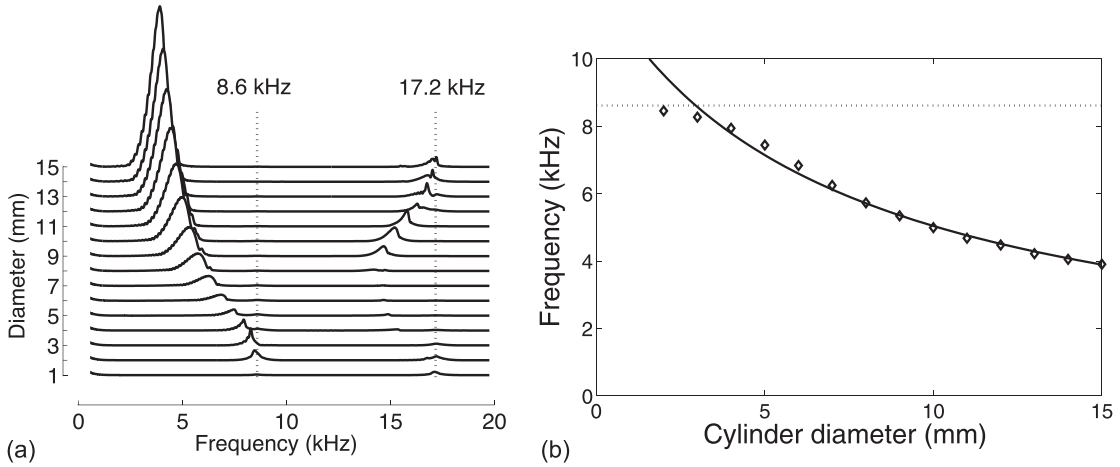

FIG. 4. Spectra of pulse tails calculated over a cylinder array with cylinder centre-to-centre spacing of 2 cm for cylinder diameters ranging from 1.0 to 15.0 mm for an input delta pulse. The source–receiver separation = 1.0 m, source and receiver heights 5 cm. Also indicated are the first and second order Bragg diffraction frequencies. (b) Variation of the frequency of the first maximum of the plots in (a) compared with the gap resonance frequencies calculated using Eq. (12b) (solid line). Also indicated is the first order Bragg diffraction frequency.

diffraction would be removed and the gap resonance frequency would be different for each inter-cylinder space of the array. However, for a fixed number of cylinders, the *average* cylinder centre-to-centre spacing for irregularly positioned cylinders would be the same as that for regularly positioned cylinders, and consequently, there would be some (significantly reduced) Bragg interference and gap resonance, depending on the spread of the cylinder centre-to-centre spacings. This is what Fig. 5 indeed demonstrates. It compares the propagation of pulses over regularly (gray line) and irregularly (black line) positioned cylinders. The first maximum, attributed to gap resonance, while significantly reduced, is not completely eliminated while the second and higher order Bragg diffraction maxima are significantly reduced, if not present.

Finally, Fig. 6 shows the variation of the magnitude of this first pulse peak generated by a cylinder array composed of 1.5 cm diameter cylinders with cylinder centre-to-centre spacing of 5 cm as a function of height. The figure shows that for receiver heights greater than 7.5 cm, the decrease in the first maximum magnitude is approximately exponential. For heights lower than this value, an interaction between neighbouring individual organ pipe resonances has not yet been achieved—as is further supported in Fig. 7. Eventually, the gap resonances merge to form an exponentially decreasing field with height, suggestive of a surface wave.

Figure 7 shows a map of the total pressure magnitude up to 10 cm above an array of twenty 1.5 cm cylinders with centre-to-centre spacing of 5 cm for five discrete frequencies: (a) 1500 Hz, (b) 2000 Hz, (c) 2500, and (d) 2782 Hz. The last frequency corresponds to the frequency of first maximum in the tail spectrum for this configuration and approximately the first minimum in the sound pressure level spectrum.

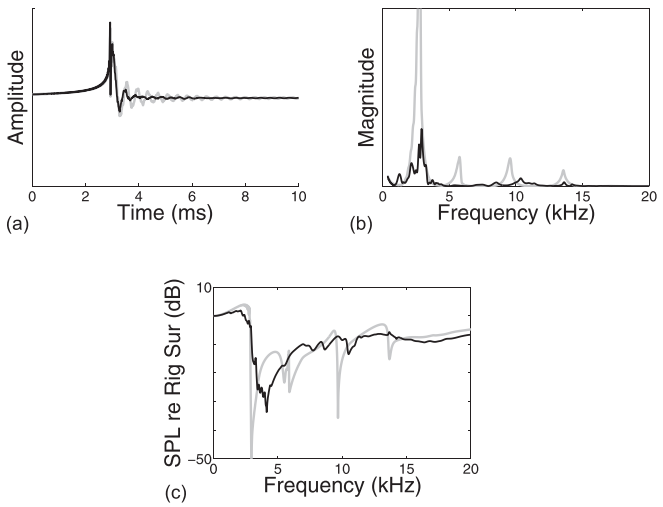

FIG. 5. Example pulse calculated for propagation of an input delta pulse over a cylinder array (1.5 cm cylinder diameter) where the cylinder centre-to-centre spacing is irregular (black line). The source–receiver separation = 1.0 m, source and receiver heights hs = hr = 5 cm. 20 cylinders are positioned at [3.6, 9.8, 12.7, 15.8, 27.9, 39.3, 42.2, 48.6, 54.7, 63.3, 65.6, 67.9, 70.7, 75.8, 79.3, 81.5, 85.0, 90.6, 93.4, 95.8] cm from the source. (a) Pulse and tail; (b) spectrum of the pulse tail; (c) sound pressure level spectrum relative to a rigid surface. This geometry and number of cylinders is the same as for Fig. 2(a) which are reproduced in this figure as the gray line for comparison.

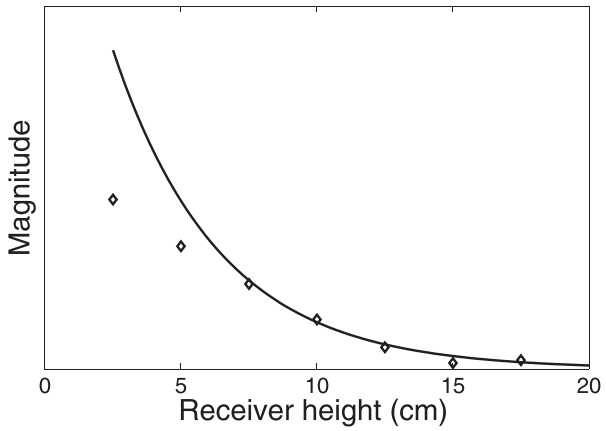

FIG. 6. Variation of the magnitude of the first maximum of the pulse tail as a function of receiver height calculated over a cylinder array with cylinder centre-to-centre spacing of 5 cm for cylinder diameter 1.5 cm for an input delta pulse. The source–receiver separation = 1.0 m, source height = 5 cm. The receiver height ranges from 2.5 to 12.5 cm. The solid line is an exponential fit for the last 5 points.

For the lowest frequency [Fig. 7(a)], the pressure magnitude demonstrates wavefront-spreading being strong close to the source and falling off towards the end of the array. As the frequency of the first tail spectrum maximum is approached, the organ pipe resonance effect starts to be excited and an increase in the pressure magnitude between the cylinders is noticeable. At 2500 Hz [Fig. 7(c)] and, in particular, at 2782 Hz [Fig. 7(d)], the inter-cylinder gap resonance is well-established, and the pressure field, while seeming to show a "standing-wave" envelope, could be considered to be confined to a region just above the cylinders. Figure 7(e) demonstrates that, when the number of cylinders is doubled thereby halving the cylinder centre-to-centre spacing, there is increasing interaction between the adjacent cylinder gap resonances.

On the basis of Figs. 6 and 7, for the geometry and cylinder configuration considered here the merging of neighbouring individual gap resonances to form a surface wave occurs some five times the cylinder diameter above the surface.

IV. MEASUREMENTS AND COMPARISON WITH THEORY

For measurements we used a surface constructed from a 1.2×2.4 m and 18 mm thick medium density fibreboard (MDF) on which were placed 0.75 m long copper cylinders (1.5 cm diameter) positioned regularly and symmetrically about the point of specular reflection at cylinder centre-to-centre spacings of 5 cm (corresponding to 20 cylinders between source and receiver). Also, the board was sufficiently plane and the cylinders sufficiently straight to avoid any acoustic leakage between cylinder and surface. All the measurements were performed in the Open University's anechoic chamber of dimensions $3\text{ m} \times 3\text{ m} \times 3\text{ m}$. The source–receiver geometry together with the cylinder array configurations were chosen to make direct comparisons with the simulations in Fig. 2.

To observe some of the main features of the pulse simulations presented in Sec. III, we selected a Ricker pulse,

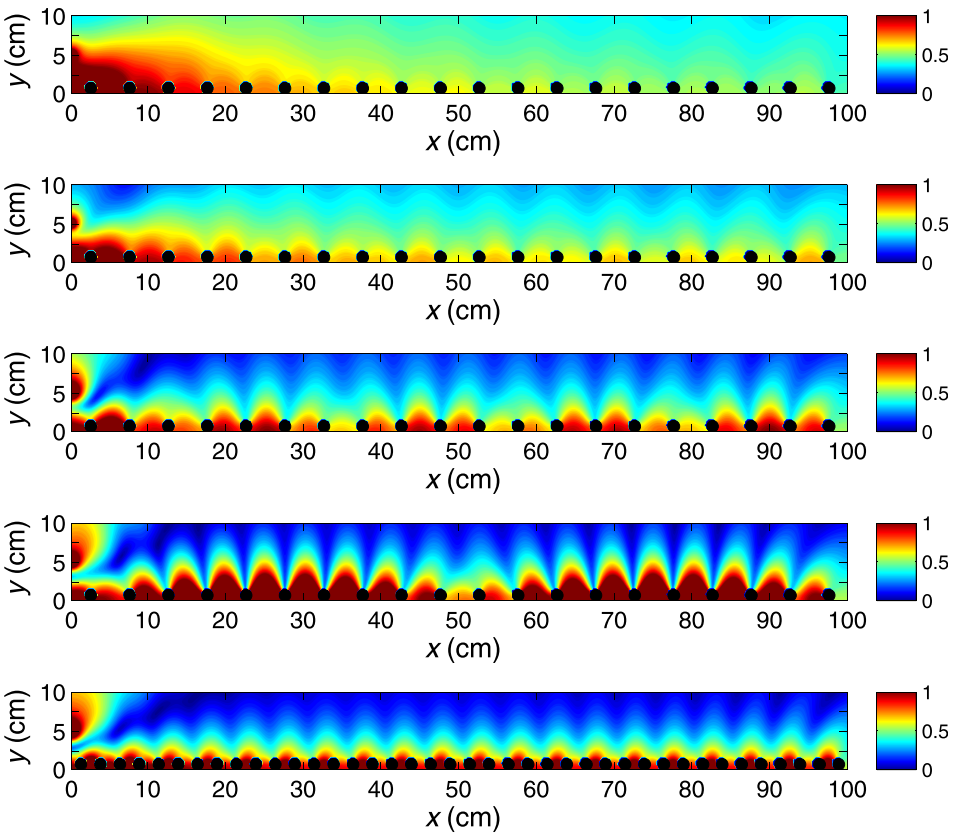

FIG. 7. (Color online) (a)–(d) Pressure maps above cylinder array with cylinder centre-to-centre spacing of 5 cm (20 cylinders), cylinder diameter 1.5 cm for an input delta pulse. The source–receiver separation = 1.0 m, the source height $y = 5$ cm ($x = 0$ cm) for the following frequencies: (a) 1500 Hz, (b) 2000 Hz, (c) 2500 Hz, and (d) 2782 Hz; (e) same source–receiver configuration, cylinder centre-to-centre spacing 2.5 cm (40 cylinders) for frequency 3169 Hz.

which has a broad frequency bandwidth, with a centre frequency of 1500 Hz for the experiments presented here. The centre frequency was selected to be sufficiently different from the frequency of the first maximum of the pulse tail for the cylinder arrays and source–receiver configurations used in the experiments. The sound source was a Tannoy driver fitted with a 2.25 m long copper tube of 3 cm internal diameter so that the end of the pipe acted as a point source at a frequency range of 400–10 kHz. A Bruel and Kjaer VR type 4311 1/2 in.-diameter condenser microphone fitted with a preamplifier was used as a receiver which has a usable sensitivity from DC to 20 kHz. Both source and receiver could be positioned with an accuracy of ∼1 mm both in the vertical and horizontal directions.

A data acquisition system based on maximum length sequence (MLS) was used for signal generation and signal processing. The signal was sampled at 75 kHz and a rectangular window of 4096 samples containing one pulse was used for the analysis. A reference signal was obtained by measuring the same pulse over the MDF board for a source height of 5 cm, a receiver height of 2.5 cm and a source–receiver separation, R, of 1 m. This geometry was selected as the first destructive interference frequency (the ground effect) was well above the frequency of interest. Thus, in the frequency range discussed here the reference sound pressure field is, in effect, double the free field. Subsequent measurements were made by placing the cylinders above the board perpendicular to source–receiver line and measuring the same sound source pulse and divided by the reference field.

Analysis was carried out on the raw time-domain signal, in particular on the component trailing the main pulse (the pulse tail). Figure 8 shows the measured (gray line) and its equivalent calculated pulse (black line), along with the pulse tail spectra and sound pressure level spectra. Given the much-reduced bandwidth and the time dependence of the input Ricker pulse, the pulse received at the microphone, together with its tail spectrum and the sound pressure level spectrum will be different from the predictions presented in Fig. 2. The pulses in Sec. III were calculated using a delta pulse with an infinite bandwidth for an idealised perfectly rigid surface with an array of cylinders of infinite length under perfect anechoic conditions. Furthermore, the finite

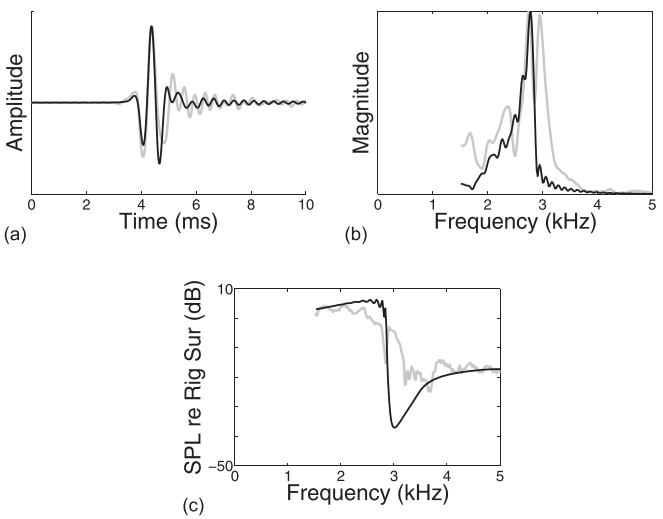

FIG. 8. (a) Example pulse, (b) its tail spectrum and (c) sound pressure level spectrum relative to a rigid surface calculated (black line) and measured (gray line) for propagation over a cylinder array configuration for an input Ricker pulse; source–receiver separation = 1.0 m, source and receiver heights = 5 cm for cylinder centre-to-centre spacing of 5 cm (20 cylinders).

size of the cylinders and board on which they were placed caused undesired reflections which influenced the pulse tail and sound pressure level spectra. For this reason, the spectra presented in Figs. 8(b) and 8(c) have been restricted to 1500 Hz to 5 kHz. Nevertheless, in both sets of data there is reasonable agreement between the data and predictions, confirming the presence of gap resonance in the pulse tail.

In their study of the propagation of pulses over lattices, Daigle *et al.*[15] found that, at source–receiver separations greater than 1.5 m, there is a clear time lag between the main arrival and the tail of ~10–15 ms. In the present study of the propagation of pulses over cylinders on a rigid surface, albeit a rather different type of rough surface, it has not been possible to demonstrate a separation of the pulse tail from the main arrival, using the multiple scattering theory even for a source–receiver separation of 2 m. This implies that the surface wave created by the cylinders on a hard plane has a speed rather close to the speed of sound in air.

V. CONCLUSIONS

Using predictions of a multiple scattering theory for propagation from a cylindrical source close to an array of cylinders on a rigid plane, it has been shown that pulses received also close to the surface are composed of a main arrival and a tail. A spectral analysis of the tail demonstrates that it is composed of regularly spaced frequency maxima that correspond to plane-wave Bragg diffraction. However, at small cylinder centre-to-centre spacings, these maxima are weak in comparison to a strong low frequency maximum related to the quarter wavelength organ pipe resonance or gap resonance in the gap between the cylinders. This resonance is enhanced with increasing cylinder diameter. Furthermore, pressure maps show that the individual resonances between neighbouring cylinders interact just above the cylinder array. With increasing heights, the merged result falls off exponentially, as is expected of a surface wave.

Finally, measurements under anechoic conditions of pulses propagating over arrays of copper tubes on a rigid fibreboard show reasonable agreement with the calculated pulses confirming the gap resonance and Bragg diffraction features present in the pulse tail.

ACKNOWLEDGMENTS

This research was developed while DLB was a Visiting Fellow at the Open University, on sabbatical leave from the University of Évora during the academic year 2017–2018; support from the Open University and the Foundation for Science and Technology (Fundação para a Ciência e a Tecnologia), Portugal, reference No. SFRH/BSAB/135168/2017, is gratefully acknowledged.

[1]B. Assouar, B. Liang, Y. Wu, Y. Li, J. C. Cheng, and Y. Ching, "Acoustic metasurfaces," Nat. Rev. Mater. **3**, 460–472 (2018).
[2]S. Thomasson, "Reflection of waves from a point source by an impedance boundary," J. Acoust. Soc. Am. **59**(4), 780–785 (1976).
[3]R. Raspet and G. E. Baird, "The acoustic surface wave above a complex impedance ground surface," J. Acoust. Soc. Am. **85**, 638–640 (1989).
[4]I. Tolstoy, "Coherent sound scatter from a rough interface between arbitrary fluids with particular reference to roughness element shapes and corrugated surfaces," J. Acoust. Soc. Am. **72**, 960–972 (1982).
[5]I. Tolstoy, "Smoothed boundary conditions, coherent low-frequency scatter, and boundary modes," J. Acoust. Soc. Am. **75**, 1–22 (1984).
[6]V. Twersky, "Reflection and scattering of sound by correlated rough surfaces," J. Acoust. Soc. Am. **73**, 85–94 (1983).
[7]K. M. Ivanov-Shits and F. V. Rozhin, "Investigation of surface waves in air," Sov. Phys. Acoust. **5**, 510–512 (1959).
[8]R. J. Donato, "Model experiments on surface waves," J. Acoust. Soc. Am. **63**, 700–703 (1978).
[9]I. Bashir, S. Taherzadeh, and K. Attenborough, "Surface waves over periodically-spaced strips," J. Acoust. Soc. Am. **134**(6), 4691–4697 (2013).
[10]W. Zhu, M. Stinson, and G. A. Daigle, "Scattering from impedance gratings and surface wave formation," J. Acoust. Soc. Am. **111**, 1996–2012 (2002).
[11]W. Zhu, G. A. Daigle, and M. Stinson, "Experimental and numerical study of air-coupled surface waves generated above strips of finite impedance," J. Acoust. Soc. Am. **114**, 1243–1253 (2003).
[12]W. Lauriks, L. Kelders, and J. F. Allard, "Surface waves above gratings having a triangular profile," Ultrasonics **36**, 865–871 (1998).
[13]L. Kelders, J. F. Allard, and W. Lauriks, "Ultrasonic surface waves above rectangular-groove gratings," J. Acoust. Soc. Am. **103**, 2730–2733 (1998).
[14]J. F. Allard, L. Kelders, and W. Lauriks, "Ultrasonic surface waves above doubly-periodic grating," J. Acoust. Soc. Am. **105**, 2528–2531 (1999).
[15]G. A. Daigle, M. R. Stinson, and D. I. Havelock, "Experiments on surface waves over a model impedance plane using acoustical pulses," J. Acoust. Soc. Am. **99**(4), 1993 (1996).
[16]I. Bashir, T. J. Hill, S. Taherzadeh, K. Attenborough, and M. Hornix, "Reduction of surface transport noise by ground roughness," Appl. Acoust. **83**(1), 1–15 (2014).
[17]K. Attenborough and S. Taherzadeh, "Propagation from a point source over a rough finite impedance boundary," J. Acoust. Soc. Am. **98**(3), 1717–1722 (1995).
[18]P. Boulanger, K. Attenborough, Q. Qin, and C. M. Linton, "Reflection of sound from random distributions of semi-cylinders on a hard plane- models and data," J. Phys. D: Appl. Phys. **38**, 3480–3490 (2005).
[19]A. Krynkin, O. Umnova, J. V Sanchez-Perez, A. Y. B. Chong, S. Taherzadeh, and K. Attenborough, "Acoustic insertion loss due to two dimensional periodic arrays of circular cylinders parallel to a nearby surface," J. Acoust. Soc. Am. **130**(6), 3736–3745 (2011).
[20]A. D. Pierce, *Acoustics: An Introduction to Its Physical Principles and Applications* (Springer International Publishing, New York, 2019).